Magn Reson Med Sci 2021; 20; 359–370
doi:10.2463/mrms.mp.2020-0009 Published Online: December 28, 2020

MAJOR PAPER

Three Dimensional Ultra-short Echo Time MRI Can Depict Cholesterol Components of Gallstones Bright

Mamoru Takahashi[1], Yasuo Takehara[2*], Kenji Fujisaki[3], Tomoyuki Okuaki[4], Yukiko Fukuma[4], Norihiro Tooyama[1], Katsutoshi Ichijo[1], Tomoyasu Amano[5], Satoshi Goshima[6], and Shinji Naganawa[7]

Purpose: Non-calcified cholesterol stones that are small in size are hard to be depicted on CT or magnetic resonance cholangiopancreatography. This institutional review board (IRB)-approved retrospective *in vitro* study aims to characterize contrast behaviors of 3 main components of the gallstones, i.e., cholesterol component (CC), bilirubin calcium component (BC) and $CaCO_3$ (CO) on 3D radial scan with ultrashort TE (UTE) MRI, and to test the capability of depicting CC of gallstones as bright signals as compared to background saline.

Methods: Fourteen representative gallstones from 14 patients, including 15 CC, 6 BC and 4 CO, were enrolled. The gallstones underwent MRI including fat-saturated T1-weighted image (fs-T1WI) and UTE MRI with dual echoes. The contrast-to-noise ratio (CNR) and the chemical analysis for the 25 portions of the stones were compared.

Results: BC was bright on fs-T1WI, which did not change dramatically on UTE MRI and the signal did not remain on UTE subtraction image between dual echoes. Whereas the CC was negative or faintly positive signal on fs-T1WI, bright signal on UTE MRI and the contrast remained even higher on the UTE subtraction, which reflected their short T2 values. Median CNRs and standard errors of the segments on each imaging were as follows: on fs-T1WI, −10.2 ± 4.2 for CC, 149.7 ± 27.6 for BC and 37.9 ± 14.3 for CO; on UTE MRI first echo, 16.7 ± 3.3 for CC, 74.9 ± 21.3 for BC and 17.7 ± 8.4 for CO; on UTE subtraction image, 30.2 ±2.0 for CC, −11.2 ± 5.4 for BC and 17.8 ± 10.7 for CO. Linear correlations between CNRs and cholesterol concentrations were observed on fs-T1WI with r = −0.885, ($P < 0.0001$), UTE MRI first echo r = −0.524 ($P = 0.0072$) and UTE subtraction with r = 0.598 ($P = 0.0016$).

Conclusion: UTE MRI and UTE subtraction can depict CC bright.

Keywords: *cholelithiasis, cholesterol gallstone, magnetic resonance, ultrashort echo time*

Introduction

Cholelithiasis or gallstone disease is prevalent with the incidence of 15% in the United States, 22% in Europe, 15% in Asia and 3% in Japan.[1–4] It can occur anywhere within the biliary trees. Most of the patients with cholelithiasis are asymptomatic and may be uneventful throughout their life; however, sometimes, it results in serious outcomes such as acute pancreatitis called gallstone pancreatitis, Mirizzi syndrome, cholecystitis or liver abscess related to cholangitis.

Gallstones are crystalline structures formed within the biliary tree by accretion or concretion of normal or abnormal bile components. There are traditional gallstone classification systems focusing on roughly three chemical components such as cholesterol component (CC), bilirubin calcium (BC) component and $CaCO_3$ (CO) component. Based on the rate of three components, gallstones are termed cholesterol stone (CS), pigmented stone (PS) and other stone (OS) (Fig. 1).[5–7]

[1]Department of Radiology, Seirei Mikatahara General Hospital, Hamamatsu, Shizuoka, Japan
[2]Department of Fundamental Development for Advanced Low Invasive Diagnostic Imaging, Nagoya University Graduate School of Medicine, Nagoya, Aichi, Japan
[3]Seirei Medical Checkup Center, Hamamatsu, Shizuoka, Japan
[4]Philips Japan, Ltd., Tokyo, Japan
[5]Department of Radiological Technology, Seirei Mikatahara General Hospital, Hamamatsu, Shizuoka, Japan
[6]Department of Diagnostic Radiology & Nuclear Medicine, Hamamatsu University School of Medicine, Hamamatsu, Shizuoka, Japan
[7]Department of Radiology, Nagoya University Graduate School of Medicine, Nagoya, Aichi, Japan

*Corresponding author: Department of Fundamental Development for Advanced Low Invasive Diagnostic Imaging, Nagoya University Graduate School of Medicine, 65, Tsurumaicho, Showa-ku, Nagoya, Aichi 466-8550, Japan. Phone: +81-52-744-2327, Fax: +81-52-744-2335, E-mail: takehara@med.nagoya-u.ac.jp

Received: January 16, 2020 | Accepted: September 10, 2020

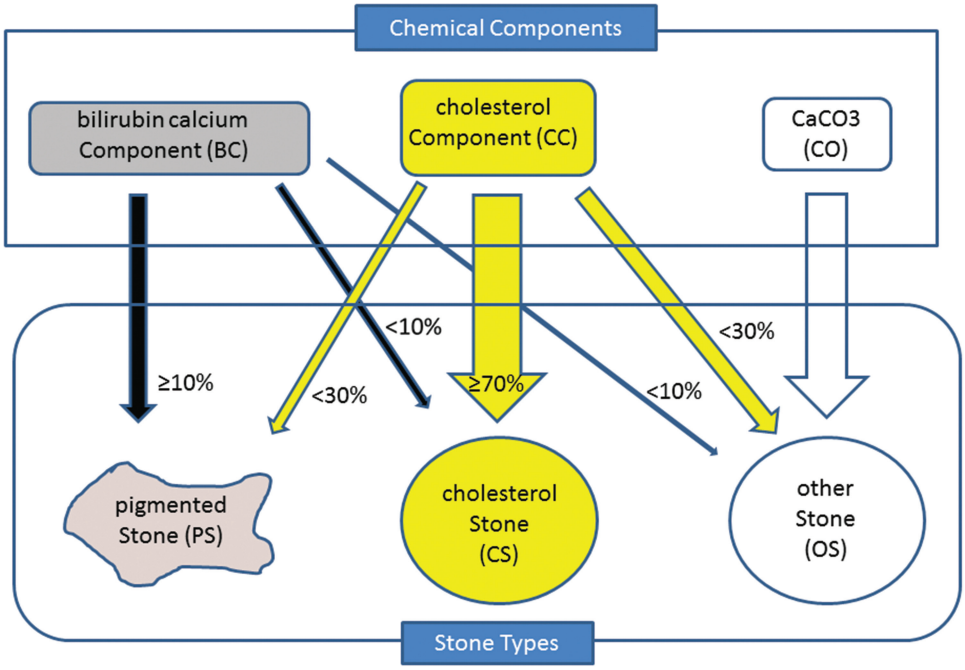

Fig. 1 A diagram showing the gallstone classification based on the ratio of three main chemical compositions. Gallstones are classified into three types of stones (i.e., PS, CS, and OS), depending on the proportion of three components, namely BC, CC, and $CaCO_3$. Stones including CC ≥ 70% were classified as CS, stones including CC < 30% and BC ≥ 10% were classified as PS and stones that do not fall into this category were classified as OS. BC, bilirubin calcium; CC, cholesterol component; CS, cholesterol stone; OS, other stone; PS, pigmented stone.

As regards the diagnosis of gallstones, endoscopic retrograde cholangiopancreatography (ERCP), MR cholangiopancreatography (MRCP), CT and ultrasonography (US) have widely been used for the diagnosis of cholelithiasis. Among them, ERCP has been postulated to be a gold standard for diagnosis of common biliary duct (CBD) stones; however, the reported incidence of post-ERCP pancreatitis is in the range of 3%–5%.[8–11] US is a handy approach and is noninvasive, whereas there are many blind corners for its detection,[12] and its diagnostic capability is dependent on the operator's skill. CT is not an appropriate tool for displaying noncalcified stones such as pure CS, because they rarely include calcium. Even with the aid of cutting edge technique of dual-energy CT, the sensitivity for the CS is around 75%–85%[13] and sometimes suffers from false positive finding of the gallstones.[14]

Although MRCP is comparable to ERCP in detecting CBD pathologies and even more accurate than CT or US,[15] its detection is dependent on heavily T2-weighted image (T2WI) that depict pathologies only as filling defects in the bright bile. The strategy of this contrast creation functions most of the occasions; however, there are several exceptional situations. One of such conditions is pneumobilia and others are hemobilia, and the most critical situation is the cholelithiasis impacted within the small intrahepatic biliary trees or narrow channel within the papilla of Vater. Since there is no bile juice surrounding the stones in such cases, the contrast between bile and the stones cannot be created on MRCP. In order to solve these drawbacks, the strategies that can depict gallstones bright are required. Fortunately, most of the PS has been reported to be hyperintense on T1-weighted image (T1WI);[16] therefore, some reports recommend that the T1WI should be combined with MRCP for improved detection of gallstones.[17] However, the bright signal of PS on T1WI is dependent on the contents of the metal chelates of the bilirubin that play the role of paramagnetic substances.[18] The strategy, therefore, cannot function in cases with pure CS that rarely contain BC.[17,18]

Susceptibility-weighted image (SWI) has recently been tested utilizing the property of diamagnetic or paramagnetic contents within the gallstones. According to Gupta et al., out of 45 surgically confirmed gallstone cases, in 43 cases, gallstones were depicted on the SWI.[19] However, the detections of CS are still challenging, because CC is diamagnetic that creates only weak susceptibility. Pneumobilia, on the other hand, creates even higher susceptibility artifacts in the biliary trees, which may be the bias in the strategy.

Instead of using the property of susceptibility, we have focused on the inherent short T2 properties of the solid-state structures of the CC. Unlike BC with loosely connected crystals, most of the CC is composed of "solid-state structure" with crystals tightly connected to each other. Conventional pulse sequences available for routine MRI are unable to create enough signals in such short T2 substances. However, recent advancement of MR technologies has enabled the application of ultrashort TE (UTE) MRI for routine clinical use. UTE MRI with 3D radial sampling of the free induction decay allows for the depiction of "solid-state" tissues or objects with very short T2 as bright signals, which help depict tendons, ligaments, menisci,[20–22] periosteum,[23] renal stones,[24] carotid plaque,[25–26] etc. Subtraction between two echoes during T2 decay makes the short T2 properties of the solid state stones more conspicuous. If this strategy is successful, CC is depicted as bright signal and may be differentiated from OS types or other soft tissue components such as biliary duct tumors on UTE MRI, which may alter the therapeutic choice.

This *in vitro* study, therefore, aims to characterize contrast behaviors of the gallstone components on UTE MRI and to test whether it can depict all gallstone components, including CC, as bright signals as compared to saline.

Materials and Methods

Patients and gallstones

The retrospective observational study carried out by the opt-out method of our website was approved by the hospital IRB (approval # 20-12).

From January 2006 to December 2008, 14 representative gallstones were sampled from 14 patients who underwent endoscopic removal, cholecystectomy or other surgical interventions (Table 1). The gallstones were rinsed with normal saline and preserved in plastic bottles to avoid the transformation of the crystalline structure by drying and were preserved in the refrigerator at around 4°C to avoid the growth of germs. The size of gallstones ranged from 4 to 20 mm with a median diameter of 10 mm. If one patient had more than one stone, the largest or representative one was adopted, because almost all gallstones in one patient were of similar kind. Fourteen gallstones were individually placed in each plastic bottle filled with normal saline, and the bottles were placed in a flat-bottomed plastic bowl half-filled with normal saline and then sent for MR imaging.

MR scanner

3.0T clinical whole body MR scanner (Ingenia 3.0T software ver. 4.1.3.0; Philips, Amsterdam, the Netherlands) with ds-Flex-M coil was used for the imaging.

Conventional fat-saturated T1-weighted image

Coronal 3D fast field echo T1WI with fat suppression (fat-saturated T1WI [fs-T1WI]) were obtained with 3D enhanced T1 high-resolution imaging with volume excitation. Parameters used were TR/TE/flip angle (FA) of 4.2 ms/1.6 ms/12 degrees, FOV of 160 mm, 164 × 162 matrix, in-plane spatial resolution of 0.99 × 0.99 mm,、slice thickness of 1.0 mm and number of signal average (NSA) of 1. The imaging time was 1 min and 53s.

3D UTE MRI

For UTE MRI, a 3D radial dual-echo sequence is applied as a scheme shown in Fig. 2. After a nonselective RF block pulse excitation, half-echo sampling starts simultaneously with gradient ramping, so that k-space is traversed from the center to outward. Radial readouts are arranged following a spiral pattern over the surface of a sphere to achieve uniform k-space coverage. From appearances, the trajectory is also called the Koosh Ball trajectory (Fig. 3). Eliminating phase encoding gradient, much shorter TE is allowed. The radial sampling covers the k-space center for all data sampling, which also allows higher signal generation.[27]

The coronal 3D radial dual-echo sequence was obtained at the first TE of 70 μs (UTE), and the second echo at 2.24 ms, where fat and water spins are in phase again. The first echo was generated with free induction decay, while the second echo was generated with a gradient echo sequence (Fig. 2). Parameters used were TR of 7.6 ms, FA of 15 degrees, FOV of 170 mm and 248 × 248 matrix. The in-plane spatial resolution was 0.69 × 0.69 mm (0.39 × 0.39 mm with zero-filled interpolation), slice thickness of 1.0 mm and NSA of 8. Double echo was obtained to enable the subtraction of the signal between two TEs. The imaging time was 8 min and 47s.

In the "dual-echo" implementation, after half-echo sampling, the readout gradient is reversed, and an additional full gradient echo is acquired. Subtraction images between the second echo and the first echo can be calculated to visualize short T2 components only.[28]

UTE MRI with multiple TE was performed to measure the T2 values when measurable. For T2 measurements, single-echo sequences with TE of 70, 100, 120 and 150 μs as well as fixed TR of 6.7 ms were used. Other parameters were the same as the above-described dual-echo UTE MRI. T2 values were calculated by fitting the T2 data to a standard exponential decay.

Macroscopic assessments of the gallstones

After imaging, all samples were cut into half pieces using surgical blade and the cut surface of the stones together with the corresponding cross sections of the fs-T1WI were macroscopically observed; the gallstones were subdivided into two to three components depending on the characteristic structures and colors (i.e., the core, the shell and the mid-layers in between） when possible. Consequently, the assessed components became 25 portions.

Table 1 Gallstone types, chemical components and appearances

No.	Stone type	Size (mm)	Form	Methods of removal	Segments	Color	Structure	Chemical component
1	CS (mosaic)	15	Ovoid	Laparoscopic Cholecystectomy	#1-1(shell)	Light brown	Laminar	CC
					#1-2(core)	Brown	Speckled	CC
2	PS	4	Ovoid	Endoscopic	#2	Black	Amorphous	BC
3	CS (mosaic)	11	Tetrahedral	Laparoscopic Cholecystectomy	#3-1(shell)	Yellowish	Laminar	CC
					#3-2(core)	Brown	Laminar	CC
4	CS (mosaic)	7	Tetrahedral	Endoscopic	#4-1(shell)	Yellowish	Laminar	CC
					#4-2(core)	Light brown	Amorphous	CC
5	PS (mosaic)	9	Ovoid	Endoscopic	#5-1(shell)	Black	Amorphous	BC
					#5-2(core)	Brown	Amorphous	CO
6	PS (mosaic)	10	Tetrahedral	Endoscopic	#6-1(shell)	Black	Laminar	BC
					#6-2(core)	Brown	Speckled	CO
7	CS (mosaic)	20	Spheric	Laparoscopic Cholecystectomy	#7-1(shell)	Dark brown	Amorphous	CC
					#7-2(core)	Brown	Amorphous	CC
8	OS	9	Tetrahedral	Endoscopic	#8	Brown	Speckled	CO
9	OS (mosaic)	17	Ovoid	Laparoscopic Cholecystectomy	#9-1(shell)	Brown	Amorphous	CO
					#9-2(core)	Light brown	Amorphous	CC
10	CS (mosaic)	12	Polygonal	Laparoscopic Cholecystectomy	#10-1(shell)	Yellowish	Radiating	CC
					#10-2(core)	Dark brown	Stellate	CC
11	PS	8	Ovoid	Endoscopic	#11	Dark brown	Laminar	BC
12	CS (mosaic)	9	Spheric	Endoscopic	#12-1(shell)	Yellowish	Laminar	CC
					#12-2(core)	Dark brown	Speckled	CC
13	CS (mosaic)	10	Ovoid	Endoscopic	#13-1(shell)	Yellowish	Laminar	CC
					#13-2(mid)	Dark brown	Laminar	BC
					#13-3(core)	Brown	Speckled	CC
14	PS	18	Oval	Lobectomy	#14	Brown	Homogeneous	BC

BC, bilirubin calcium; CC, cholesterol; CO, $CaCO_3$; CS, cholesterol stone; OS, other stone; PS, pigmented stone.

Chemical composition analysis and typing of the gallstones

Using half pieces, the gallstones as a whole were classified into three groups according to the rate of chemical contents of CC and BC (Fig. 1). Our classification is based on the traditional scheme classifying gallstones into three types according to chemical composition. Stones including CC ≥ 70% was classified as CS, stones including CC < 30% and BC ≥ 10% were classified as PS and stones that do not fall into this category were classified as OS (5–7).

Using the remaining half pieces of the gallstones, subdivided 25 segments underwent subsequent chemical analysis. The analysis was performed in the external laboratory (SRL, Tokyo, Japan) in a blinded fashion. Each part of gallstones was pulverized and desiccated to constant weight. Dried gallstone powder was then extracted with acidified methanol−chloroform mixture (1:1; v/v). The insoluble material (residue) was desiccated to dry weight and was not analyzed further. The segments of the gallstones were then chemically analyzed. The concentrations of CC (%), BC (%), CO (%) and calcium (mgCa/g) concentrations were measured by infrared absorption spectrometry (KBr tablet method).

Signal measurement of the gallstones

Contrast-to-noise ratios (CNR) of all 25 segments of the gallstones on fs-T1WI, UTE (1st echo) and UTE (2nd echo) were measured. On each contrast, mean signal

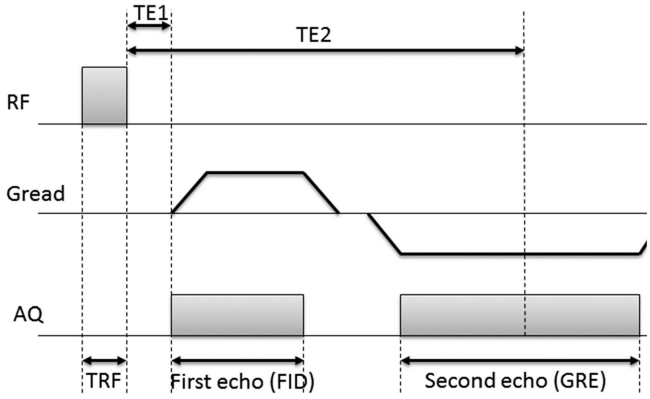

Fig. 2 A pulse sequence diagram of the 3D ultra-short TE "dual-echo" radial sequence. After a TRF block pulse excitation, half-echo sampling (first echo) starts simultaneously with gradient ramping, so that k-space is traversed from the center to outward. Radial readouts are arranged following a spiral pattern over the surface of a sphere to achieve homogeneous k-space coverage. The first echo was generated with free induction decay, while the second echo was generated with a gradient echo sequence. A later full gradient echo (second echo) is acquired at TE2, which is chosen to be first water/fat in-phase TE. On eliminating the phase encoding gradient, shorter TE is available in this particular data sampling. AQ, acquisition window; FID, free induction decay; GRE, gradient echo; TRF, tailored RF.

intensity of the three compartments of the gallstones (i.e., CC, BC and CO) were measured by placing ROIs (median pixels of 73, ranging from 12 to 292 pixels) on the gallstones, adjacent surrounding saline outside the containers and the standard deviation of a largest circular ROI outside the container. All measurements were repeated three times performed by two radiologists (Y. T. and M.T.) independently, and the values were averaged. For a quantitative assessment, CNRs for gallstone to the surrounding saline were calculated as follows: CNR (average signal of gallstone – average signal of surrounding saline) background noise.

Statistics

The differences of CNRs between groups were assessed with nonparametric Kruskal–Wallis test. If the Kruskal–Wallis test was positive ($P < 0.05$), then a test for pairwise comparison of subgroups according to Dunn–Bonferroni analysis was performed. The scattergram was created to compare signals on T1WI, UTE MRI and UTE subtraction images. The relationships between CNRs and chemical compositions on each segment were compared on the scattergram. Nonparametric Spearman's coefficient of rank correlation (rho) test was performed and the P values were calculated. Statistical application (MedCalc ver. 14.10.2; MedCalc, Ostend, Belgium) was used for the analysis. P values less than 0.05 were considered significant.

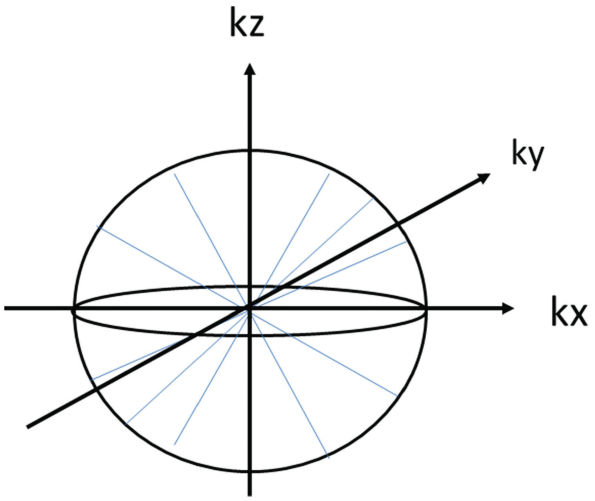

Fig. 3 The scheme of data sampling trajectories in the k-space for 3D UTE radial sequence, which is called "Koosh Ball" trajectory. Each data lines include the k-space center, which is a low frequency portion that creates a high signal. UTE, ultra-short TE.

Results

Based on the chemical contents of the CC and BC (Fig. 1), 14 gallstones were classified into 7 CS, 5 PS and 2 OS. Ten out of 14 gallstones were the mosaics of segments with different colors and characteristic mixed contrasts on fs-T1WI. The gallstones were visually assessed and segmented into 25 parts. Based on the chemical analysis, the segments were known to be composed of 15 CC, 6 BC and 4 CO portions (Table 1). Macroscopically, CC was mostly laminar, radiating or speckled structure with yellowish color. BC was characterized by mostly amorphous or homogeneous structure with colors of dark brown to black color and CO was amorphous or speckled structures with brown color (Table 1).

The contrast behaviors of BC-dominant portions were bright on fs-T1WI and the contrast did not change dramatically on UTE MRI as compared to fs-T1WI. In addition, the signal did not remain on UTE subtraction image (Fig. 4a–4d). The CC dominant portions, on the contrary, were negative or faintly positive signal on fs-T1WI, bright signal on UTE MRI and the conspicuous contrast remained on UTE subtraction image, which reflected its short T2 values (Fig. 5a–5d). The stone with mosaic components composed of BC and CC revealed laminar or speckled patterns of contrast reflecting each segment (Fig. 6a–6d).

Median CNRs and standard errors for each gallstone segments on each imaging were as follows: on fs-T1WI, -10.2 ± 4.2 for CC, 149.7 ± 27.6 for BC and 37.9 ± 14.3 for CO (Fig. 7a); on UTE first echo, 16.7 ± 3.3 for CC, 74.9 ± 21.3 for BC and 17.7 ± 8.4 for CO (Fig. 7b); on UTE subtraction image, 30.2 ± 2.0 for CC, -11.2 ± 5.4 for BC and 17.8 ± 10.7 for CO (Fig. 7c).

Significant linear correlations between CNRs of each gallstone segments and cholesterol concentrations were observed on

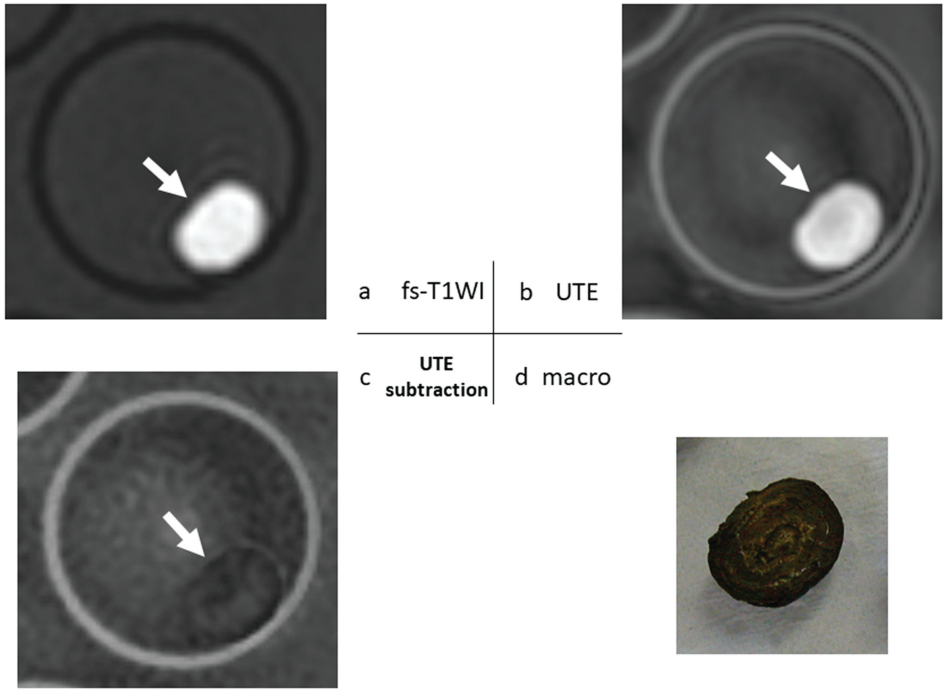

Fig. 4 The MR contrast behavior of a pigmented stone containing 13% cholesterol and 77% bilirubin calcium (stone #11). (**a**) On fs-T1WI, the stone shows homogeneous bright signal (arrow) as compared to surrounding saline. (**b**) On UTE MRI, almost similar contrast is shown (arrow). (**c**) On UTE subtraction, only a faint signal remains, which reflects most of the stone consisted of long T2 crystals (arrow). (**d**) Macroscopic appearance of the corresponding cross section of the stone. Dark brown laminar structures characterize the nature of rich bilirubin calcium component. fs-T1WI, fat-saturated T1-weighted imaging; UTE, ultrashort TE.

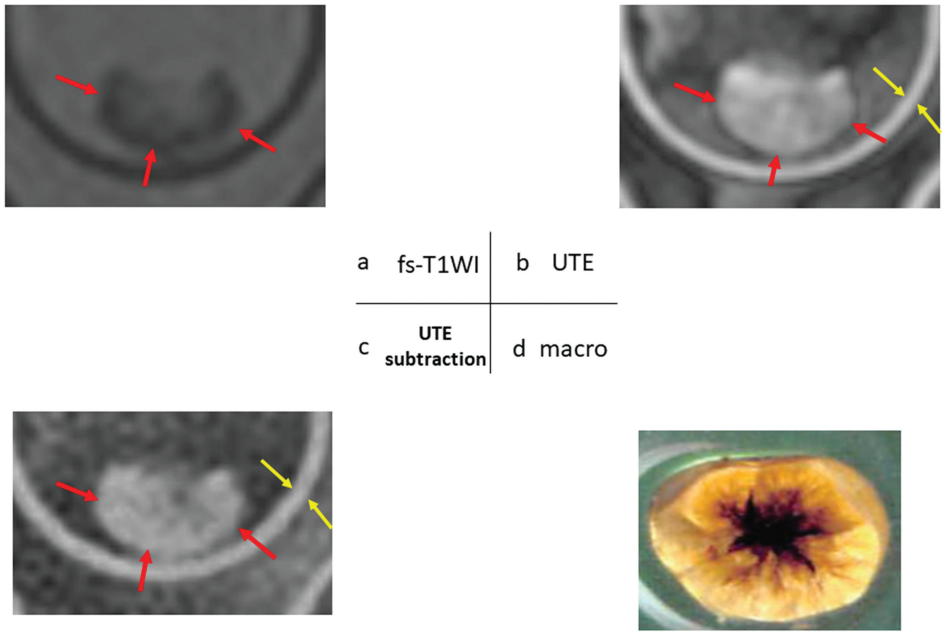

Fig. 5 The stone consisted of 97% cholesterol and 3% bilirubin calcium and was classified into a cholesterol stone as a whole (stone #10). (**a**) On fs-T1WI, negative signal (red arrows) is observed as compared to surrounding saline. (**b**) On UTE-MRI, the stone is depicted as a higher signal (red arrows) as compared to saline. Note that plastic bottle is also depicted as a bright signal on UTE images (yellow arrows). (**c**) UTE subtraction image creates a conspicuous bright signal reflecting short T2 property of the gallstone (red arrows). The signal of the plastic bottle also remains (yellow arrows). (**d**) Macroscopic appearance of the corresponding cross section of the stone. The characteristic yellowish appearance reflects rich cholesterol crystals with central stellate crack with faint pigmentation are seen. fs-T1WI, fat-saturated T1-weighted imaging; UTE, ultrashort TE.

fs-T1WI with r = −0.885 (CI: −0.949, −0.754) ($P < 0.0001$), UTE first echo r = −0.524 (CI: −0.762, −0.163) ($P = 0.0072$) and UTE subtraction with r = 0.598 (CI: 0.265, 0.803) ($P = 0.0016$) (Fig. 8a). Similarly, the CNRs of each gallstone segments were significantly correlated to BC concentration on fs-T1WI with r = 0.662 (CI: 0.362, 0.838) ($P = 0.0003$), UTE first echo r = 0.550 (CI: 0.198, 0.776) ($P = 0.0044$) and subtraction with r = −0.613 (CI: −0.812, −0.288) ($P = 0.0011$) (Fig. 8b). The correlation between CNR on fs-T1WI and calcium content was r = 0.750 (CI: 0.504, 0.883) ($P < 0.0001$) (Fig. 8c).

Cholesterol concentration of each gallstone segments were inversely correlated to calcium content with r = −0.755 (CI: −0.886, −0.513) ($P < 0.0001$).

CNR on UTE vs. calcium content: r = 0.342 (CI: −0.0620, 0.649) ($P = 0.0947$) and CNR on subtraction vs. calcium content: r = −0.326 (CI: −0.639, 0.079) ($P = 0.116$) were not significant.

T2 properties of the gallstones were measurable for 12 CC and 4 CO, with median ± SE of 65.8 ± 10.4 μs ranging from 48.2 to 160 μs (Fig. 9a–9e).

Discussion

Current diagnostic performance of MRCP for the choledocholithiasis is comparable to ERCP or even better than that of CT or US with reasonable sensitivities of 85%–100%, specificities of 90%–99%.[12,13] However, detection of intrahepatic stones or impacted stones in a cystic duct or a duodenal papilla is still challenging, because high signal intensity bile is lacking around the low signal intensity stones. Likewise, gas bubbles are occasionally encountered in the biliary duct (pneumobilia), which are recognized as round low intensity on T2WI and may cause false positive for a diagnosis of gallstones.[29–31] The flow void of the bile may also cause pseudolesions.[29–31] These drawbacks can be overcome if there is a pulse sequence allowing even a fraction of the gallstones, which is depicted as a bright signal. Since some gallstones are reported to be hyperintense on T1WI, T1WI in combination with T2WI can help avoid these pitfalls.[16,32–34] Nevertheless, the strategy works out only for PS and some OS including paramagnetic metal

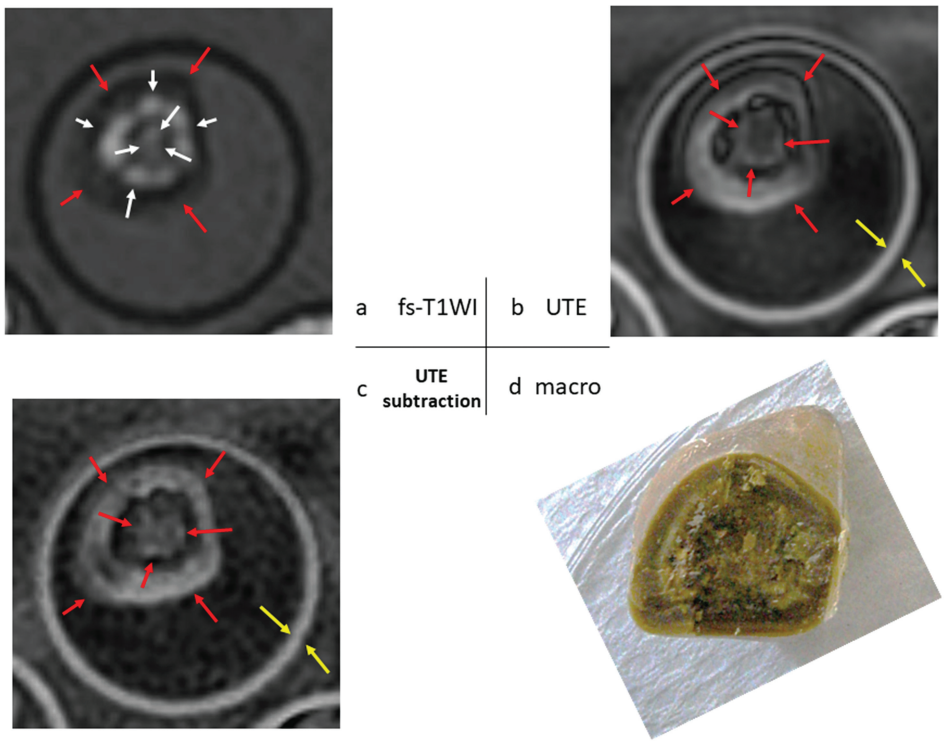

Fig. 6 Cholesterol stone (stone #13) including a shell of almost pure cholesterol component, whereas the inner layer and the portion of the core consist of abundant and small amount of BC, respectively. As shown in the images, the combination of fs-T1WI and subtraction images can characterize the heterogeneous nature of this gallstone. (**a**) On fs-T1WI, BC (the portion of the core and the inner layer) (white arrows) are depicted as bright signals, whereas CC (the shell and the most of the core) (red arrows) are negative signals as compared to surrounding saline signal. (**b**) On the UTE MRI, the CC layers and the most of the core are depicted (red arrows) as bright signal. The wall of the plastic bottle is also bright (yellow arrows). (**c**) The contrast conspicuity of the, CC portions, is increased on UTE subtraction. Note that solid-state portions i.e., CC (red arrows) and the wall of the plastic bottle (yellow arrows), are bright signals. (**d**) Macroscopic appearance of the corresponding cross section. Multilayers of yellowish CC and the mixture of BC in between are shown as dark brown. BC, bilirubin calcium; CC, cholesterol component; fs-T1WI, fat-saturated T1-weighted imaging; UTE, ultrashort TE.

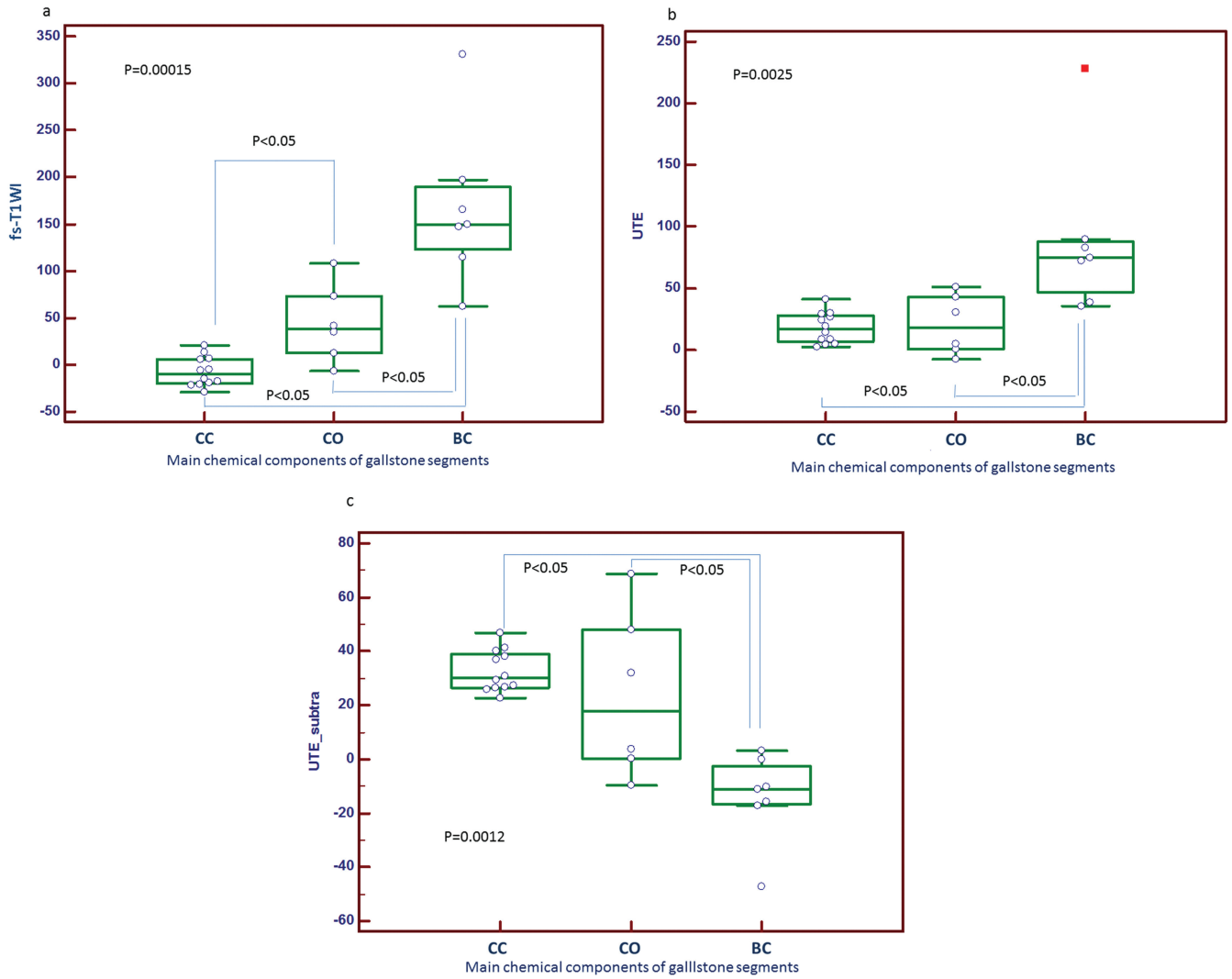

Fig. 7 Box-Whisker plots of CNRs of the gallstone segments on each imaging are shown. (**a**) On fs-T1WI, segments composed mainly of CC is negative to faintly positive CNRs; however, the segments composed mainly of BC shows conspicuously high CNRs. The CNRs are −10.2 ± 4.2 for CC, 37.9 ± 14.3 for CO and 149.7 ± 27.6 for BC. (**b**) On UTE first echo, the CNRs of the segments composed mainly of CC turn positive; the CNRs are 16.7 ± 3.3 for CC, 17.7 ± 8.4 for CO and 74.9 ± 21.3 for BC. (**c**) On UTE subtraction image, the segments composed mainly of CC shows even higher CNRs (30.2 ± 2.0), whereas CNRs for most of the BC turn negative (−11.2 ± 5.4). BC, bilirubin calcium; CC, cholesterol component; CNRs, contrast-to-noise ratios; CO, carbonate component; fs-T1WI, fat-saturated T1-weighted imaging; UTE, ultrashort TE.

chelates and usually not for CS.[17,18] Indeed, we have observed that all BC appeared distinctly positive signal on fs-T1WI; whereas, 9 out of 15 CC were faintly positive or negative signal on fs-T1WI. Besides the differences of the amount of paramagnetic metal ion content between BC and CC, the crystal structures are different between these two. BC shows loose and fragile structures with relatively more water contents. CC, on the other hand, has more solid-state ultrastructures formed by tightly bound cholesterol crystals. Because molecular motion is restricted in the solid-state objects, T2 relaxation time is markedly shortened due to the spin–spin interactions. Using ordinary MR sequences, shortest TE is limited around 1 ms at shortest. After alpha pulse, the transverse magnetizations within CC decay rapidly during ordinary TE and disappearance of the signals follows.[35] Unlike ordinary pulse sequences, UTE MRI can detect such short T2 components before echo signals decay. Using UTE of 70 μs, short T2 properties of CC that are within the range of 45.4–160 μs could create bright signals on UTE MRI (Figs. 5b, 6b, 9a).[20] The UTE subtraction well highlighted the contrast between two types of stone components reflecting their differences of solid-state ultrastructures (Figs. 5c, 6c, 10).

The differential diagnosis between CS and PS is sometimes clinically important because the information may change the therapeutic decisions.[36–39] Normally, PS can easily be crushed by a mechanical lithotripter and retrieved irrespective of its size. In contrast, the big CS are harder and sometimes non-breakable, which may cause the endoscopic lithotripsy

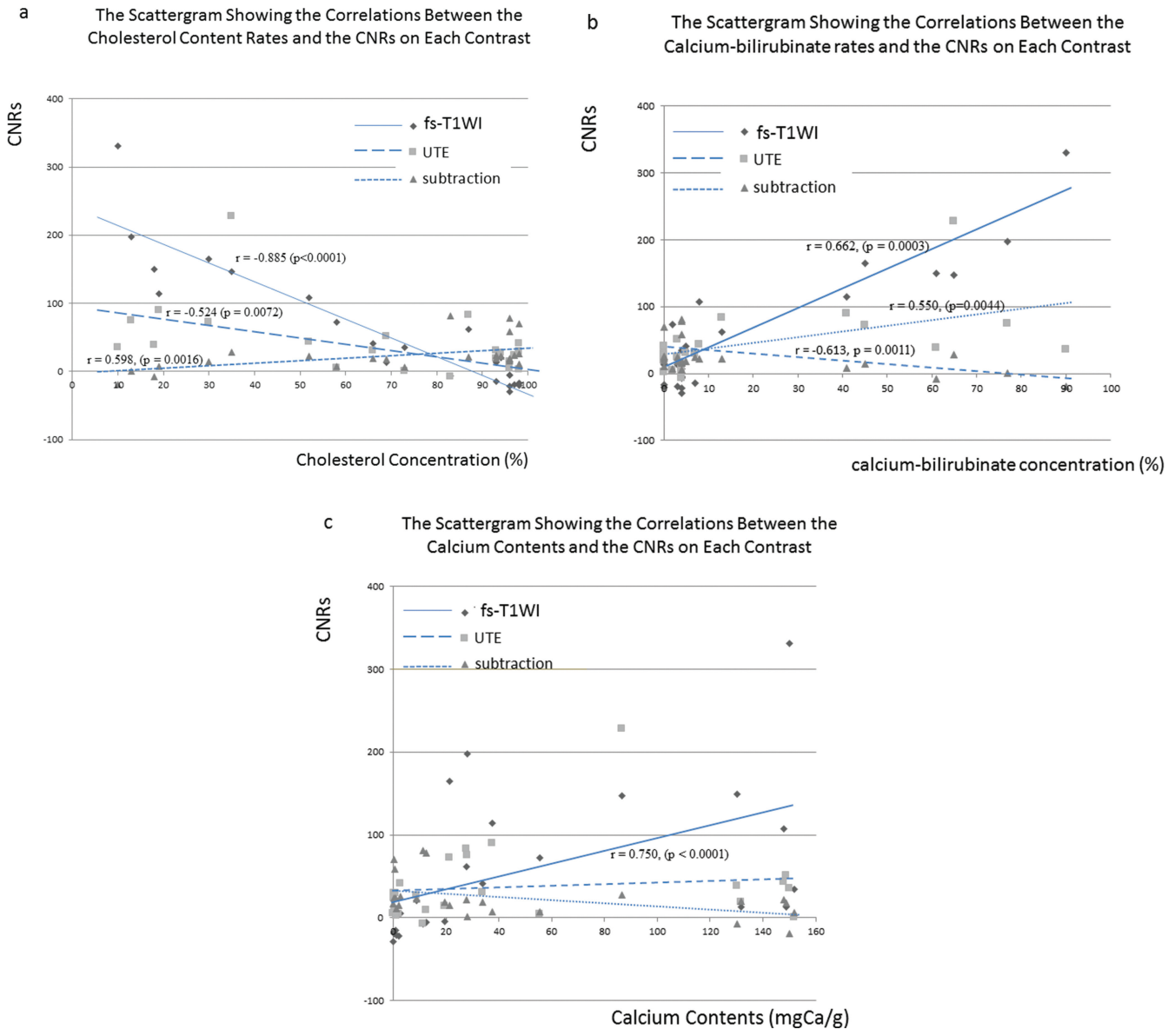

Fig. 8 (**a**) Significant linear correlations between CNRs of the gallstone segments and cholesterol concentrations were observed on fs-T1WI with r = −0.885 (CI: −0.949, −0.754) ($P < 0.0001$), UTE first echo r = −0.524 (CI: −0.762, −0.163) ($P = 0.0072$) and UTE subtraction with r = 0.598 (CI: 0.265, 0.803) ($P = 0.0016$). (**b**) Similarly, CNRs of the gallstone segments were significantly correlated to bilirubin calcium contents on fs-T1WI with r = 0.662 (CI: 0.362, 0.838) ($P = 0.0003$), UTE first echo r = 0.550 (CI: 0.198, 0.776) ($P = 0.0044$) and subtraction with r = −0.613 (CI: −0.812, −0.288), $P = 0.0011$). (**c**) The correlation between CNRs of the gallstone segments and calcium content was seen on fs-T1WI with r = 0.750 (CI: 0.504, 0.883) ($P < 0.0001$). CNRs, contrast-to-noise ratios; fs-T1WI, fat-saturated T1-weighted imaging; UTE, ultrashort TE.

maneuver to fail.[17,40] UTE MRI may be useful in differentiating CS from PS or OS. Unlike PS or OS, CS is a negative or a faintly positive signal on fs-T1WI and bright on UTE subtraction. CC may also be differentiated from PS or OS by the calcium content. The indication of current bile acid dissolution therapy has been based on CT, in which density less than 60–100 HU (i.e., CC) are indicated.[38,41,42] Given the CNR on conventional fs-T1WI is also proportional to the calcium content (Fig. 8c), fs-T1WI may be used in place of CT in estimating the calcium content of the gallstones.

To summarize our results, a scheme shown in Fig. 10 may help understand the relationship between stone types, chemical contents, signal on fs-T1WI and UTE subtraction and the crystal types or T2 values.

This study is not free from potential limitations. First, the study may be affected by a bias of limited sample size. As a stone basis, we only had seven CS, five PS and two OS. Second, the *in vitro* study may not entirely warrant the performance in the clinical environments. For instance, MR has limited spatial resolution for the

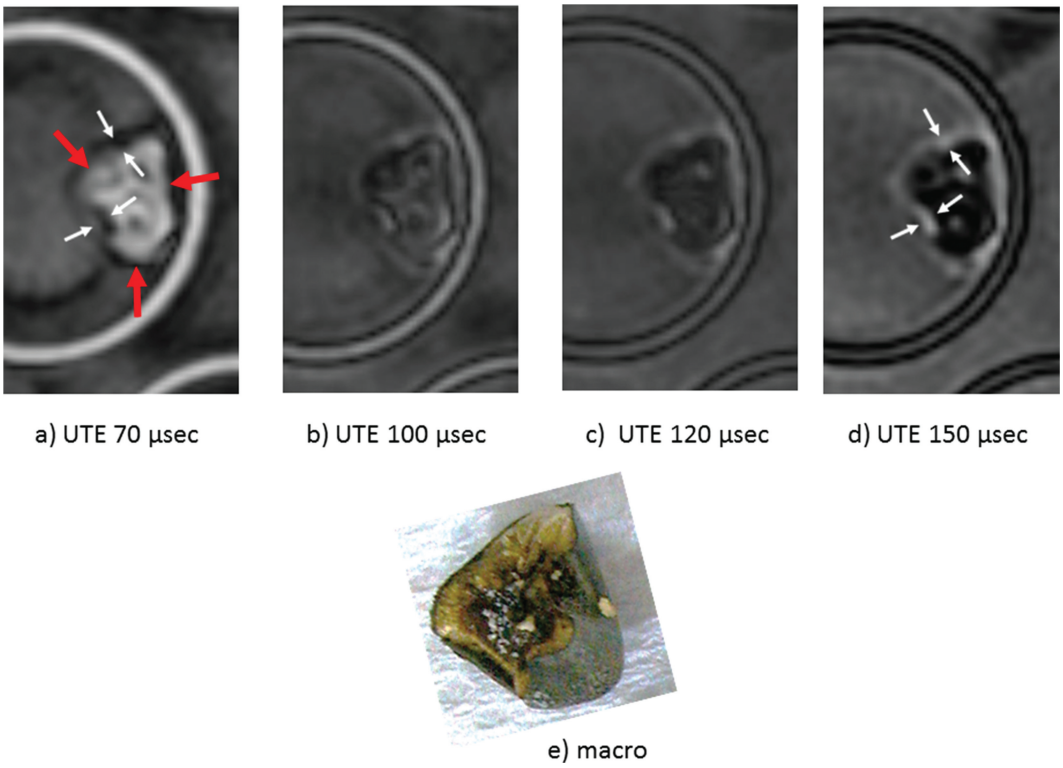

Fig. 9 UTE MRI for a gallstone containing 73% cholesterol (most of the central part) and 3% bilirubin calcium (outer cortical layer) and was classified into the cholesterol stone as a whole (stone #1). The contrast of the CC varies depending on the variable TEs ranging from (**a**) 70 µs, (**b**) 100 µs, (**c**) 120 µs and (**d**) 150 µs. Note that TE less than 100 µs is required to depict CC portion (red arrows) as bright signal as compared to surrounding normal saline. To the contrary, the thin cortical layer of the BC (white arrows on **a** and **d**) with high signal on longer TE shows signal loss at shorter TE. (**e**) Macroscopic appearance of the corresponding cross section. The stone consists mostly of CC and a small amount of BC in the thin cortex. BC, bilirubin calcium; CC, cholesterol component; UTE, ultrashort TE.

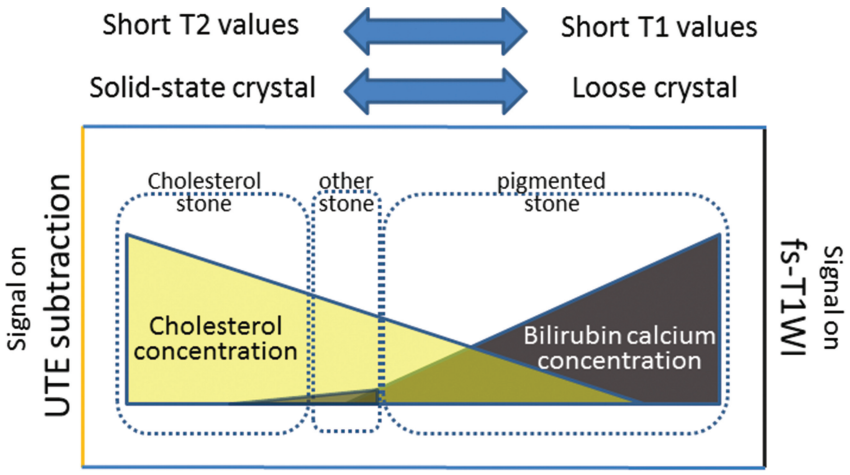

Fig. 10 A scheme showing the relationship of stone signal on fs-T1WI and UTE subtraction, chemical components and stone types. All gallstones (cholesterol stones, pigmented stones and other stones) are categorized based on the concentration of two main chemical substances (cholesterol and bilirubin calcium). To summarize the signal behavior of gallstones on fs-T1WI and UTE subtraction, the signal is proportional to bilirubin calcium concentration on fs-T1WI, and the signal on UTE subtraction is proportional to cholesterol concentration. Short T2 values of the cholesterol crystals are mainly due to the solid state of the cholesterol crystals. Short T1 values on fs-T1WI are dependent on the paramagnetic metal bilirubin in the pigmented stones. fs-T1WI, fat-saturated T1-weighted imaging; UTE, ultrashort TE.

tiny gallstones, and moreover, the imaging time for current 3D Fourier transform (FT) UTE MRI is lengthy for breath-holding imaging, which may affect the assessment of the small stones. The potential use of 2D FT UTE MRI under breath-holding imaging may solve this limitation. The third limitation is the signal reference for the stones used in this study. We compared the signal of gallstones with surrounding saline; however, in the real world, the contrast must be created by the signal between gallstones with adjacent bile sometimes concentrated, sometimes with the mixture of hemobilia or pneumobilia. Lastly, we have measured the CNRs of subsegments of the gallstones instead of gallstones as a whole, which may not reflect exactly the same conspicuity of the gallstones. However, the gallstones are mostly mosaics of chemically different segments, and we therefore deem that the detection of the gallstones is still feasible when just a portion of the stone is bright.

Although more extended clinical study is required to confirm our results, the study implicates that the combined use of conventional fs-T1WI and UTE subtraction image may be helpful in depicting all gallstones not even encircled by bile fluid as bright signal and that the differentiation of CS from PS or OS might be allowed solely with MRI without ionizing radiation.

Conclusion

In conclusion, UTE MRI and UTE subtraction image have shown an added value in depicting all gallstones including CS as a bright signal (higher than surrounding saline), which may promise the improved differentiation and detection of gallstones on MRI.

Conflicts of Interest

Corresponding author Yasuo Takehara is an endowed chair of Nagoya University Graduate School of Medicine, supported by a private company. Tomoyuki Okuaki and Yukiko Fukuma are employees of Philips Japan Ltd. The other coauthors have no conflict of interest.

References

1. Aerts R, Penninckx F. The burden of gallstone disease in Europe. Aliment Pharmacol Ther 2003; 18; Suppl 3:49–53.
2. Everhart JE, Khare M, Hill M, et al. Prevalence and ethnic differences in gallbladder disease in the United States. Gastroenterology 1999; 117:632–639.
3. Misciagna G, Leoci C, Guerra V, et al. Epidemiology of cholelithiasis in southern Italy. Part II: Risk factors. Eur J Gastroenterol Hepatol 1996; 8:585–593.
4. Stinton LM, Shaffer EA. Epidemiology of gallbladder disease: Cholelithiasis and cancer. Gut Liver 2012; 6:172–187.
5. Sato T, Kameda H. Panel discussion (1): Indication of silent stones for surgery. Proceedings of the 65th Annual Meeting of the Japanese Society of Gastroenterology 1979, Tokyo, Japan. Gastroenterol Jpn, 1979; 14:631–649.
6. Qiao T, Ma RH, Luo XB, et al. The systematic classification of gallbladder stones. PLoS One 2013; 8:e74887.
7. Ravnborg L, Teilum D, Pedersen LR. Gallbladder stones classified by chemical analysis of cholesterol content. Frederiksberg, 1987–1988. Scand J Gastroenterol 1990; 25:720–724.
8. Cooper ST, Slivka A. Incidence, risk factors, and prevention of post-ERCP pancreatitis. Gastroenterol Clin North Am 2007; 36:259–276, vii–viii.
9. Kochar B, Akshintala VS, Afghani E, et al. Incidence, severity, and mortality of post-ERCP pancreatitis: A systematic review by using randomized, controlled trials. Gastrointest Endosc 2015; 81:143–149.e9.
10. Murray WR. Reducing the incidence and severity of post ERCP pancreatitis. Scand J Surg 2005; 94:112–116.
11. Nicholson JA, Greenhalf W, Jackson R. Incidence of post-ERCP pancreatitis from direct pancreatic juice collection in hereditary pancreatitis and familial pancreatic cancer before and after the introduction of prophylactic pancreatic stents and rectal diclofenac. Pancreas 2015; 44:260–265.
12. Gupta M. Gastrointestinal imaging, In: Pickhardt PJ, eds. Gastroenterology clinics of North America. Philadelphia:Elsevier, 2018; 585–602.
13. Lee HA, Lee YH, Yoon KH, et al. Comparison of virtual unenhanced images derived from dual-energy CT with true unenhanced images in evaluation of gallstone disease. AJR Am J Roentgenol 2016; 206:74–80.
14. Yoshida R, Yoshizako T, Katsube T, et al. Computed tomography findings of ceftriaxone-associated biliary pseudocholelithiasis in adults. Jpn J Radiol 2019; 37:826–831.
15. Baillie J, Paulson EK, Vitellas KM. Biliary imaging: A review. Gastroenterology 2003; 124:1686–1699.
16. Safar F, Kamura T, Okamuto K, et al. Magnetic resonance T1 gradient-echo imaging in hepatolithiasis. Abdom Imaging 2005; 30:297–302.
17. Tsai HM, Lin XZ, Chen CY, et al. MRI of gallstones with different compositions. AJR Am J Roentgenol 2004; 182:1513–1519.
18. Ukaji M, Ebara M, Tsuchiya Y, et al. Diagnosis of gallstone composition in magnetic resonance imaging: *in vitro* analysis. Eur J Radiol 2002; 41:49–56.
19. Gupta RK, Neelavalli J, Gupta M, et al. Evaluation of gall bladder stones using susceptibility weighted imaging. J Comput Assist Tomogr 2019; 43:747–754.
20. Gatehouse PD, Bydder GM. Magnetic resonance imaging of short T2 components in tissue. Clin Radiol 2003; 58:1–19.
21. Gold GE, Pauly JM, Macovski A, et al. MR spectroscopic imaging of collagen: Tendons and knee menisci. Magn Reson Med 1995; 34:647–654.
22. Rahmer J, Bornert P, Dries SP. Assessment of anterior cruciate ligament reconstruction using 3D ultrashort echo-time MR imaging. J Magn Reson Imaging 2009; 29:443–448.
23. Reichert IL, Benjamin M, Gatehouse PD, et al. Magnetic resonance imaging of periosteum with ultrashort TE pulse sequences. J Magn Reson Imaging 2004; 19:99–107.

24. Ibrahim el SH, Cernigliaro JG, Pooley RA, et al. Detection of different kidney stone types: An ex vivo comparison of ultrashort echo time MRI to reference standard CT. Clin Imaging 2016; 40:90–95.
25. Du J, Corbeil J, Znamirowski R, et al. Direct imaging and quantification of carotid plaque calcification. Magn Reson Med 2011; 65:1013–1020.
26. Du J, Peterson M, Kansal N, et al. Mineralization in calcified plaque is like that of cortical bone—further evidence from ultrashort echo time (UTE) magnetic resonance imaging of carotid plaque calcification and cortical bone. Med Phys 2013; 40:102301.
27. Wong ST, Roos MS. A strategy for sampling on a sphere applied to 3D selective RF pulse design. Magn Reson Med 1994; 32:778–784.
28. Yassin A, Pedrosa I, Kearney M, et al. *In vitro* MR imaging of renal stones with an ultra-short echo time magnetic resonance imaging sequence. Acad Radiol 2012; 19:1566–1572.
29. David V, Reinhold C, Hochman M, et al. Pitfalls in the interpretation of MR cholangiopancreatography. AJR Am J Roentgenol 1998; 170:1055–1059.
30. Sugita R, Sugimura E, Itoh M, et al. Pseudolesion of the bile duct caused by flow effect: A diagnostic pitfall of MR cholangiopancreatography. AJR Am J Roentgenol 2003; 180:467–471.
31. Watanabe Y, Dohke M, Ishimori T, et al. Diagnostic pitfalls of MR cholangiopancreatography in the evaluation of the biliary tract and gallbladder. Radiographics 1999; 19:415–429.
32. Choi IY, Yeom SK, Cha SH, et al. Diagnosis of biliary stone disease: T1-weighted magnetic resonance cholangiography with Gd-EOB-DTPA versus T2-weighted magnetic resonance cholangiography. Clin Imaging 2014; 38:164–169.
33. Erden A, Haliloglu N, Genc Y, et al. Diagnostic value of T1-weighted gradient-echo in-phase images added to MRCP in differentiation of hepatolithiasis and intrahepatic pneumobilia. AJR Am J Roentgenol 2014; 202:74–82.
34. Kim YK, Kim CS, Lee JM, et al. Value of adding T1-weighted image to MR cholangiopancreatography for detecting intrahepatic biliary stones. AJR Am J Roentgenol 2006; 187: W267–274.
35. Baron RL, Shuman WP, Lee SP, et al. MR appearance of gallstones *in vitro* at 1.5 T: Correlation with chemical composition. AJR Am J Roentgenol 1989; 153:497–502.
36. Bilhartz LE. Cholesterol gallstone disease: The current status of nonsurgical therapy. Am J Med Sci 1988; 296:45–56.
37. Bowen JC. Gallstone disease: Current therapy. Semin Ultrasound CT MR 1993; 14:321–324.
38. Pereira SP, Veysey MJ, Kennedy C et al. Gallstone dissolution with oral bile acid therapy. Importance of pretreatment CT scanning and reasons for nonresponse. Dig Dis Sci 1997; 42:1775–1782.
39. Portincasa P, Ciaula AD, Bonfrate L, et al. Therapy of gallstone disease: What it was, what it is, what it will be. World J Gastrointest Pharmacol Ther 2012; 3:7–20.
40. Lim JH, Kim KW, Choi D. Chapter 31: Biliary tract and gallbladder, In: Haaga JR, eds. Computed tomography & magnetic resonance imaging of the whole body. 5th ed. Philadelphia, PA:Mosby, 2008; 1378.
41. Caroli A, Del Favero G, Di Mario F, et al. Computed tomography in predicting gall stone solubility: A prospective trial. Gut 1992; 33:698–700.
42. Petroni ML, Jazrawi RP, Grundy A, et al. Prospective, multicenter study on value of computerized tomography (CT) in gallstone disease in predicting response to bile acid therapy. Dig Dis Sci 1995; 40:1956–1962.